Microstructure evolution of gold thin films under spherical indentation for micro switches contact applications

Brice Arrazat, Vincent Mandrillon, Karim Inal, Maxime Vincent, Christophe Poulain

Microstructure evolution of gold thin films under spherical indentation for micro switches contact applications

Brice Arrazat*[1,2], Vincent Mandrillon[1,2], Karim Inal[1], Maxime Vincent[2,3], Christophe Poulain[2]

[1] Packaging and Flexible Substrate, Ecole Nationale Supérieure des Mines de Saint-Etienne, Armines, Centre de Microélectronique de Provence - Georges Charpak, Gardanne, France
[2] Microsystems Characterization and Reliability Lab., CEA - Léti, Minatec, Grenoble, France
[3] Innovation Division, Schneider Electric Industries, Grenoble, France

* Corresponding author: Phone +33 4 42 61 67 57, fax +33 4 42 61 65 93 and e-mail address arrazat@emse.fr

Abstract

RF MEMS (Radio Frequency Micro Electro Mechanical System) switches are promising devices but their gold-on-gold contacts, assimilated for this work to a sphere / plane contact, represent a major reliability issue. A first step towards failure mechanism understanding is the investigation of the contact metal microstructure evolution under static and cyclic loading. After static and cyclic loading of sputtered gold thin films under spherical indentation, high resolution Electron Back Scatter Diffraction (EBSD) is used to investigate contact area. Grain rotation against {111} fiber texture of 1 µm thick sputtered gold thin film is a signature of plastic deformation. Grain rotation is observed above 1.6 mN under static loading by a spherical diamond indenter with 50 µm tip radius. A heterogeneity in grain rotation is observed corresponding to a more important plastic deformation in the middle of the indent than at the edge. A 30° Grain rotation is observed for a half million mechanical cycles under 300 µN load by a spherical gold tip (20 µm radius) due to cyclic work hardening. The same test in hot switching mode induces a grain growth in the contact area. Therefore thermal effects occurring during hot switching are underlined.

Keywords: micro-switch reliability, EBSD, microstructure, nano-indentation, contact mechanics.

---

1. Introduction

Regarding the large spectrum of telecommunication standards and demands of communicating objects, transceiver systems will be dynamically reconfigurable. The most common possibility by far consists in a switching matrix to direct the signal through a dedicated block. For that possibility, the Micro Electro Mechanical Systems (MEMS) switch is an attractive alternative to traditional FET (Field Effect Transistor) or p-i-n diode switches in applications where microsecond-switching speed is sufficient. A MEMS switch is composed by a mobile part (bridge or beam) and a contact area of few µm² (flat or spherical bump) separated by an air gap (Figure 1). The mechanical movement obtained using electrostatic, magnetostatic, piezoelectric, or thermal actuation is necessary to close the switch. These components show much lower insertion loss and higher isolation than their competitors [1].

Recent works on contact switch reliability revealed two primary failure mechanisms during cycling which are contact resistance increase and stiction [2, 3]. Those mechanical degradations of contact are linked to contact material properties. Practically, gold is selected as the contact material due to low resistivity and low sensitivity to oxidation. But, gold's relative low hardness and low softening temperature seem to be the origin of contact degradation [2, 3].

To solve this problem, several studies are dedicated to alternative contact materials [2-4]. Gold alloyed with platinum-group metals are preferentially considered. Significant results are obtained showing sevenfold lifetime increases [3]. But the same failure mechanisms occur. To understand the mechanisms which are at the origin of contact degradation, some investigations on morphology integrity are performed. Yan et al [5] demonstrate that degradation area increases with current intensity increase (from 70 to 350 mA). Also, degradation area increases under mechanical cycling at a force of 200 µN as a function of the number of cycles and is linked to an increase in contact resistance [6]. Gregori investigates the deformation in the contact area and shows that partial flattening of asperities and pile-up formation occur with actuation [7]. Curvature radius of asperities and mechanical

properties (elasticity and hardness) of material are major parameters of adhesion force [8] and the evolution of adhesion force could explain stiction mode of failure.

In this work, after static and cyclic loading of sputtered gold thin films under spherical indentation, high resolution Electron Back Scatter Diffraction (EBSD) is used to investigate contact area microstructural changes. Complementary Atomic Force Microscopy (AFM) topography characterization (pile-up, indent diameter, asperity curvature radius) of contact area is performed. Localized nanoindentation measurement of hardness evolution linked to observed structural changes is also performed.

2. Samples description

Sample consists of the following sputtered thin film stack deposited on a silicon substrate: 1µm of gold / 50 nm tungsten nitride diffusion barrier / 20 nm tungsten adhesion layer. The rms roughness of the investigated gold surface is 5 nm. The average peak-to-valley is 35 nm. The average curvature radius of asperities on gold thin film is 240 nm.

Recent studies [9] have demonstrated the maturity of EBSD in field emission scanning electron microscope (FEGSEM). High spatial resolution is reached as small as 10 nm. Penetration depth is around 5 nm into gold thin films. Crystallographic texture and grain boundary rotation of surface are determined and quantified. A strong {111} fiber texture normal to the gold surface is exhibited with an average 90nm grain size.

A Nanoindenter XP from MTS instruments is used to determine mechanical properties of the gold thin film using the dynamic contact module (DCM) option using a Berkovich indenter tip. The continuous stiffness measurement (CSM) technique allows the measurement of dynamic stiffness continuously throughout the loading segment by superimposing a small dynamic oscillating displacement to the quasi-static force by means of a frequency-specific amplifier. The oscillation displacement was 1 nm, the frequency was 50 Hz and the strain rate was constant (0,05 s^{-1}). The area function of the Berkovich tip was obtained by the indentations on fused silica in the range of 10–300 nm indentation depth, i.e. displacement as suggested by [10]. A total of 64 indentations were conducted on gold thin film and the average values of 64 indentations are presented in Figure 9. At a depth of 150 nm, the hardness of the gold thin film is 1.6 GPa and the elastic modulus is 80 GPa.

3. Mechanical solicitations

In this study, using the nanoindenter, ten static loads ranging from 50µN up to 130mN are applied on the gold thin film at different locations with a spherical diamond tip of 50µm radius to be representative of micro-switch contact pressure (Table 3). These experiments proceed as follow: after surface contact, the load increases with a constant strain rate (0,05 s^{-1}). The targeted load is applied during 1 second, then unload occurs at the same strain rate.

To perform mechanical cycling in the same pressure range, an apparatus (Vincent [11]) for endurance testing in both hot and cold switching mode under constant voltage is used. In cold switching mode, the voltage between the probe and the gold film is only applied when the switch is closed, while the voltage is always applied in hot switching mode leading to closure and opening electrical effects. This apparatus is constituted by a commercial ferromagnetic reed blade (flexible beam) where the sample is glued and put into contact with a 20 µm curvature radius gold probe using a piezoelectric actuator having a displacement resolution of 10 nm as shown in Figure 1. The applied load is measured using a strain gage force sensor with 20 µN resolution. After first contact and load adjustment, an electromagnet located above the ferromagnetic beam is used for cyclic contact opening / closing actuation under sinusoidal excitation. Load, switching frequency, voltage and current compliance are respectively fixed to 300µN, 10 Hz, 5 V and 1 mA (Table 2).

In order to have a comparison criterion between the mechanical solicitations under static loading, cyclic loading and a real micro-switch, the equivalent average contact pressure (P_{eq}) corresponding to the applied load F is introduced and calculated from Hertz equation for a sphere / plane elastic contact (Eq. 1).

$$P_{eq} = \frac{1}{\pi}\left(\frac{4E_{eq}}{3R}\right)^{2/3} F^{1/3} \qquad \mathbf{1}$$

E_{eq} and R are respectively the effective elastic modulus and curvature radius of indenter tip. The former being related to material properties by the following relationship:

$$\frac{1}{E_{eq}} = \frac{1-\upsilon_i^2}{E_i} + \frac{1-\upsilon_f^2}{E_f} \qquad \mathbf{2}$$

E and υ are Young's modulus and Poisson's ratio, subscripts f and i corresponding respectively to the film and to the indenter tip. Young's modulus and Poisson's ratio value for the gold thin film are E_f=80 GPa (experimental) and v_f=0.44. The calculated effective elastic modulus for the different spherical indenter types are collected Table 1.

	E_i (GPa)	v_i	R (µm)	E_{eq} (GPa)
Gold-on-gold micro-switch	80	0.44	~10	49.6
Spherical indenter (static)	1140	0.07	50	91.3
Spherical gold probe (cyclic)	80	0.44	20	49.6

Table 1 : Young's modulus, Poisson's ratio and radii of different indenter types and their effective elastic modulus.

In the following part of the article the hertzian equivalent average contact pressure is always used. Load applied in a micro switch is about 10 µN. Therefore, for a contact bump curvature radius of 10 µm, the MEMS switch pressure is around 240 MPa. Endurance cycling experiments are carried out at 470 MPa (Table 2). On different test areas, 26 thousands and a half million cycles are respectively performed in hot and cold switching mode (Table 2).

Cycling conditions	Hot switching (5V, 1mA, 10Hz)	Cold switching (5V, 1mA, 10Hz)
Cyclic loading (mN)	0.3	0.3
Pressure (MPa)	470	470
Number of cycles	26 000	500 000

Table 2 : Cyclic loading, calculated pressure and number of cycles of tests performed.

Static loads applied by spherical indentation are summarized Table 3. The range of MEMS switch pressure is investigated at low loads. At high loads, pressures above 1 GPa allow a high degradation analysis but obviously does not corresponds to the real applied pressure due to contact plastic deformation.

Static loading (mN)	0,05	0,22	0,55	1	1,6	7	18	37	73	130
Pressure (MPa)	210	350	470	580	670	1100	1500	1920	2410	2920

Table 3 : Static loads and calculated pressures applied by spherical diamond indentation (radius 50 µm).

4. Static loading analysis

Geometry of the residual indent mark created under static loading (Table 3) at contact location is determined by AFM measurement. The diameter and depth of spherical indent and pile-up height are defined Figure 2. The indent depth (h) is defined as the difference between reference plane and bottom of indent. The pile-up height (s) is defined as the difference between the top of pile-up and reference plane. A gaussian filter is used to remove the short wavelength components as shown Figure 2. The diameter of the residual imprint obtained during indentation increases with applied pressure (Figure 3). It is observed that this increase of diameter follows the classic plastic model [12], where the hardness equals the ratio between the load and the projected contact area, such as the hardness equals 1 GPa. The experimental data and plastic model are represented Figure 3 respectively by points and a red line. The pile-up formation is observed above 500 MPa (Figure 5). The ratio (s/h) of pile-up height on indent depth increases from 0 to 0.5 with pressure applied. This is due to the transition from purely elastic deformation at low pressure to plastically dominated behavior at high pressure [13]. The pile-up is a signature of thin film global plastic deformation.

Experimentally, indent marks created under pressures lower than 400 MPa are difficult to quantify. Only some asperities are partially hammered. The limit of detection corresponds to Tabor condition where plastic deformation starts over third part of hardness. Around 500 MPa, the roughness in the center of indent is around 4 nm and close to gold thin film value of 5 nm. When the pressure increases above 500MPa, the roughness decreases drastically to less than 2 nm due to plastic deformation. Before solicitation the average curvature radius of asperities on gold thin film is around 240 nm. Above 500 MPa of applied pressure, the average curvature radius of the asperities in the middle of the indent is of 850 nm showing huge plastic deformation of

asperity summits added to global plastic deformation. The same evolution of the roughness and of the curvature radius of asperity after twelve millions cycles under 180 µN in [7] is found corresponding to an increase propensity to permanent adhesion.

The previous indents, already analyzed by AFM, are investigated by EBSD characterization as shown Figure 6. Comparison of both images demonstrates the one to one equivalency between topographic asperities with the grain shapes observed by EBSD. As previously shown, gold thin film has a strong {111} fiber texture. The grain circled Figure 6 at the middle of the indent mark obtained under a 1.6 mN static load suffers 10 degrees of rotation in comparison to the {111} initial fiber texture. Only grains in the middle of indent present a rotation. Therefore observed deformation is heterogeneous. Thus a 1x1µm² area is analyzed for each indent to determine average grain rotation as a function of average pressure. No grain size modification is observed on any indent. Rotation angle of grains increases with pressure above 500MPa (Figure 5). This rotation reaches 21° under an equivalent pressure of 3GPa. The ratio (s/h) of pile-up height on indent depth and the grain rotation follow the same evolution with applied pressure and are representative of the level of plastic deformation (Figure 5).These rotations induce the {111} fiber texture degradation. Central spot and external fringe on {111} pole figure are larger. In extreme cases, central spot transforms in new circle. This type of crystallographic texture deformation is also observed on polycristals under uniaxial compression [14]. This grain reorientation can be predicted by Taylor-type model of crystalline plasticity [14].

This demonstrates that EBSD analysis gives precious information on plastic deformation level. Therefore, this characterization technique will be applied on cyclic loading contact areas with interest.

5. Cyclic loading mode analysis

A half million cold switching cycles is performed as detailed Table 2. The setup of this experiment needs a first contact approach with the piezoelectric actuator. This first contact force is around 1 mN and induces a grain rotation of 10° (Figure 7-c). After the approach, mechanical cycling under a 300 µN load is performed by the sinusoidal signal send to the electromagnet. A grain rotation of 30° is observed after a half million cycles. This is due to cumulative plastic deformation. The grain rotation obtained is higher than under 3 GPa static loading contact pressure. The {111} Pole figure obtained has a strong crystallographic texture and is slightly different from static loads. First contact approach induces a shift of the {111} texture fiber. Then, mechanical cycling induces larger central spot and external fringe on the {111} pole figure.

A single indentation in the degradation area is performed (Figure 9). The measured hardness increases by 12% on a half million quasi cold switching cycles area at a 150 nm of depth. No grain size modification was observed on a half million quasi cold switching area. Therefore the measured hardness increase is due to strain hardening.

The same test is performed in hot switching mode. Grain Boundary rotation obtained for 26,000 hot switching cycles is around 25°, that is, of the same order than after a half million cycles cold switching experiment. Moreover, resulting crystallographic texture of the contact area is extremely different from previous tests. A strong degradation of the {111} fiber texture is observed but no particular orientation is predominant (Figure 7-d). The grain size has increased in contact area. The average grain size is around 250 nm, whereas initial average grain size of gold thin film is around 90 nm. Thermal energy produced during by hot switching (arcing or melting) induces an abnormal recrystallization. The grain size increase and the resulted crystallographic texture differ from previous solicitations and is the expression of a different mechanism of degradation.

A single indentation in the degradation area is also performed. At a depth of 150 nm, the measured hardness decreases by 22% compared to the initial gold thin film. This decrease of hardness could correspond to the Hall-Petch effect described by the following relation,

$$H = H_0 + K_H d^{-1/2} \qquad \mathbf{3}$$

Where H_0 and K_H are experimental constant and d is the average grain size (equation 3). More experiments in hot switching mode should be addressed to use this relation. A comparison with the results obtained in Cao study [15] concerning the decrease of gold hardness with grain size is presented Figure 10.

6. Conclusions

The interest of EBSD analysis for micro-switch reliability study is demonstrated through this work. We have highlighted the following points:

- The {111} pole figure evolution shows grain rotation due to plastic deformation, with good correlation with pile-up intensity.
- The {111} pole figure gives information about the type of solicitation: compression.
- The grain size determined by EBSD leads to the confirmation that thermal events occuring during hot switching are strong enough to concern the all grain volume and to induce grain growth.
- The hardness measurements are coherent with microstructural evolution observed by EBSD.

Others points should be addressed to improve EBSD analysis and will be implemented into further studies. First, a crystallographic plastic model can be used to predict microstructural evolution, and secondly this type of analysis will be performed on the contact area of a real micro switch.

References

[1] G.M. Rebeiz and J.B. Muldavin. Rf mems switches and switch circuits. *Microwave Magazine, IEEE*, 2(4):59–71, Dec 2001.

[2] R. A. Coutu, P. E. Kladitis, L. A. Starman, and J. R. Reid. A comparison of micro-switch analytic, finite element, and experimental results. *Sensors and Actuators A: Physical*, 115(2-3):252–258, September 2004.

[3] R.A. Coutu, J.R. Reid, R. Cortez, R.E. Strawser, and P.E. Kladitis. Microswitches with sputtered au, aupd,au-on-aupt, and auptcu alloy electric contacts. *Components and Packaging Technologies, IEEE Transactions on*, 29(2):341–349, June 2006.

[4] L. Chen, H. Lee, Z. J. Guo, N. E. McGruer, K. W. Gilbert, S. Mall, K. D. Leedy, and G. G. Adams. Contact resistance study of noble metals and alloy films using a scanning probe microscope test station. *Journal of Applied Physics*, 102(7):074910, 2007.

[5] X. Yan, N.E. McGruer, G.G. Adams, and S. Majumder. Finite element analysis of the thermal characteristics of mems switches. *TRANSDUCERS, Solid-State Sensors, Actuators and Microsystems, 12th International Conference on, 2003*, 1:412–415 vol.1, June 2003.

[6] L. Chen Z.J. Guo Y. Du N.E. McGruer, G.G. Adams. Mechanical, thermal, and material influences on ohmic-contact-type mems switch operation. *IEEE MICROWAVE MAGAZINE*, 2006.

[7] Giuliano Gregori and David R. Clarke. The interrelation between adhesion, contact creep, and roughness on the life of gold contacts in radio-frequency microswitches. *Journal of Applied Physics*, Volume 100 / Issue 9, 2006.

[8] P.Y. Duvivier, V. Mandrillon K. Inal. Time dependence investigation of the electrical resistance of Au / Au thin film micro contacts. *Holm Conference on Electrical Contacts*, in press

[9] F. J. Humphreys. Review grain and subgrain characterisation by electron backscatter diffraction. *Journal of Materials Science*, Volume 36, Number 16, 2001.

[10] G. M. Pharr, J. H. Strader, and W. C. Oliver. Critical issues in making small-depth mechanical property measurements by nanoindentation with continuous stiffness measurement. *JOURNAL OF MATERIALS RESEARCH*, 24(3):653–666, MAR 2009. International Symposium on Indentation Behavior of Materials, Hyderabad, INDIA, FEB, 2008.

[11] M. Vincent, L. Chiesi, P. Rousset, C. Lapiere, C. Poulain, L. Carbone, F. Houze, and J. Delamare. An original apparatus for endurance testing of mems electrical contact materials. *Electrical Contacts, 2009 Proceedings of the 55th IEEE Holm Conference*, pages 288 – 292, September 2009.

[12] Anthony C. Fischer-Cripps. *Nanoindentation*. 2004.

[13] G.M. Pharr B. Taljat. Development of pile-up during spherical indentation of elastic–plastic solids. *International Journal of Solids and Structures*, 41:3891–3904, 2004.

[14] S. R. Kalidindi C. A. Bronkhorst and L. Anand. Polycrystalline plasticity and the evolution of crystallographic texture in fcc metals. *Phil. Trans. R. Soc. Lond.*, 341:443–477, 1992.

[15] Yifang Cao, Seyed Allameh, Derek Nankivil, Steve Sethiaraj, Tom Otiti, and Wole Soboyejo. Nanoindentation measurements of the mechanical properties of polycrystalline au and ag thin films on silicon substrates: Effects of grain size and film thickness. *Materials Science and Engineering: A*, 427(1-2):232 – 240, 2006.

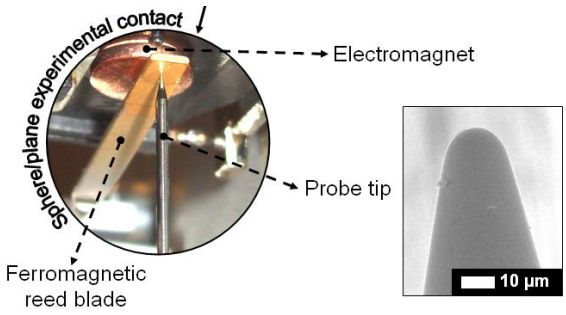

Figure 1 : Apparatus dedicated to cyclic loading test.

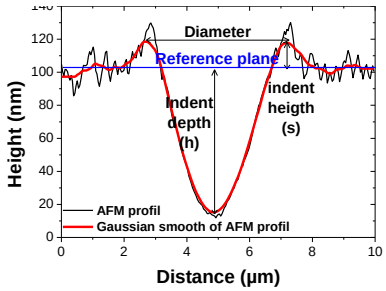

Figure 2 : Typical AFM profile of one of the hole created during indentation.

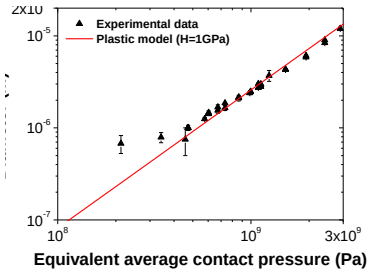

Figure 3 : Diameter versus equivalent pressure (Pa) of spherical indentation (50µm tip radius) in gold thin film.

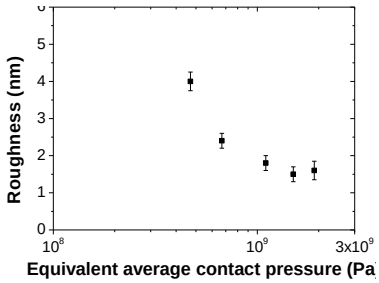

Figure 4 : Root mean square roughness in the middle of the indent mark versus applied pressure after static loading spherical indentation.

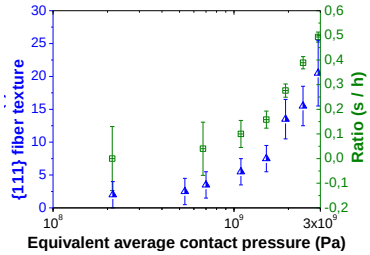

Figure 5 : Ratio s/h between height of pile-up and indent depth, and grain rotation relative to {111} fiber texture as a function of equivalent average contact pressure (Pa) of spherical indentation (50µm radius) in the gold thin film.

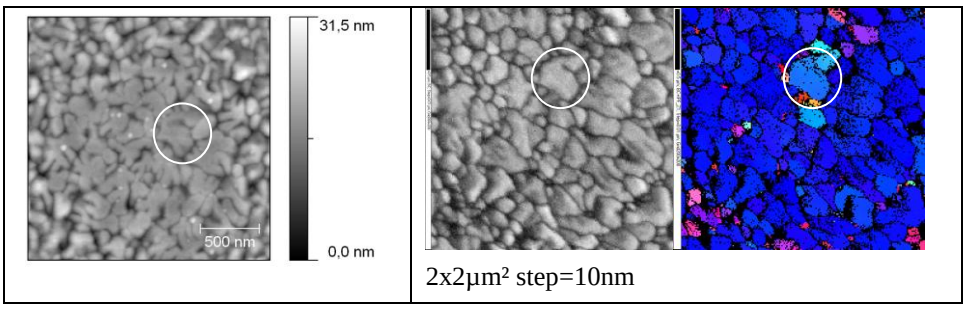

Figure 6 : Flattened top view of indent mark at 1,6mN static load. Circled grain shows a 10° rotation due to contact. Grains in red were already disoriented before contact.

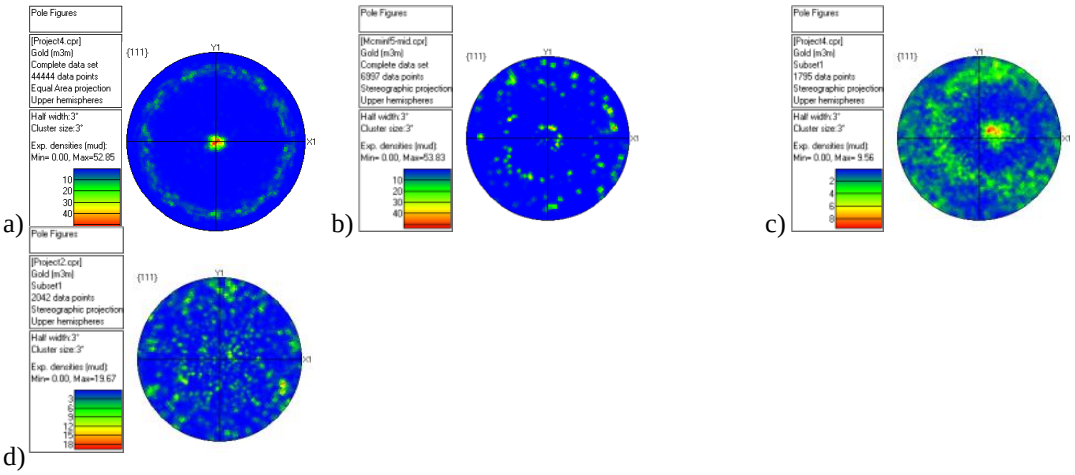

Figure 7 : {111} pole figure of initial gold thin film (a), after a 73 mN static loading (b), after half million cold switching cycles under 300 µN (c) and after 26 thousand hot switching cycles under 300 µN (d).

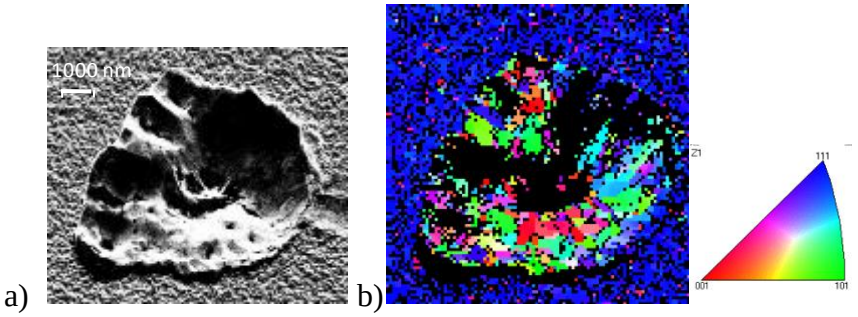

Figure 8 : Scanning Electron Microscopy image (a) and EBSD map (b) of 26 thousand hot switching cycles contact area under 300 µN load.

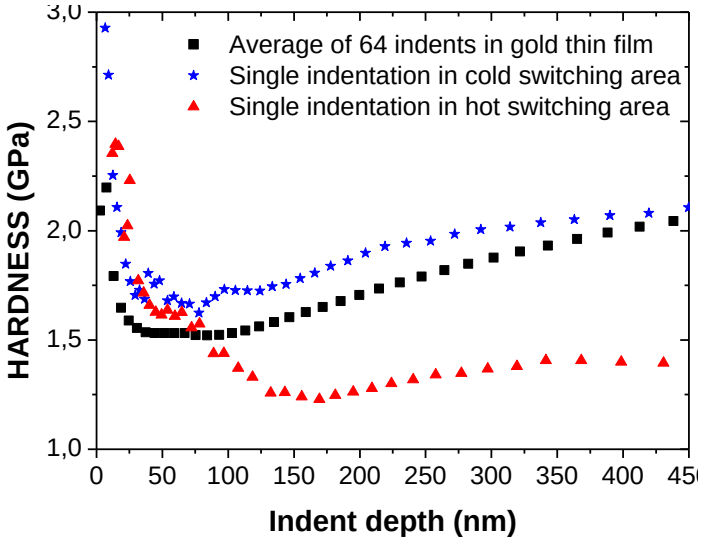

Figure 9 : gold thin film hardness measurement as a function of depth before and after contact loading.

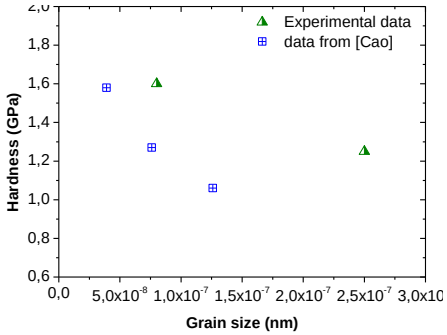

Figure 10 : Measured Hardness versus grain size.